Draft version October 29, 2010
Preprint typeset using LaTeX style emulateapj v. 11/10/09

EXTREMAL ENERGY SHIFTS OF RADIATION FROM A RING NEAR A ROTATING BLACK HOLE

Vladimír Karas, and Vjačeslav Sochora
Astronomical Institute, Academy of Sciences, Boční II 1401, CZ-14131 Prague, Czech Republic
Draft version October 29, 2010

ABSTRACT

Radiation from a narrow circular ring shows a characteristic double-horn profile dominated by photons having energy around the maximum or minimum of the allowed range, i.e. near the extremal values of the energy shift. The energy span of a spectral line is a function of the ring radius, black hole spin, and observer's view angle. We describe a useful approach to calculate the extremal energy shifts in the regime of strong gravity. Then we consider an accretion disk consisting of a number of separate nested annuli in the equatorial plane of Kerr black hole, above the innermost stable circular orbit (ISCO). We suggest that the radial structure of the disk emission could be reconstructed using the extremal energy shifts of the individual rings deduced from the broad wings of a relativistic spectral line.
Subject headings: galaxies: nuclei — black hole physics — accretion, accretion disks

1. INTRODUCTION

Emission from inner regions of accretion disks around black holes provides wealth of information about matter in extreme conditions. Relativistic spectral line of iron, broadened and skewed by fast orbital motion and redshifted by strong gravitational field, has been used to constrain the parameters of the black hole, both in active galactic nuclei (AGN; Fabian et al. 2000; Reynolds & Nowak 2003; Miller 2007) and Galactic black holes (Miller et al. 2002; McClintock & Remillard 2006). During recent years, much discussion has revolved round the question of how close to the innermost stable circular orbit (ISCO, also called the marginally stable orbit, $r = r_{\rm ms}$; Misner et al. 1973) the accretion disk extends, whether the line is produced all the way down to the inner edge, and if the emission from the accretion disk can be approximated by a smooth radial profile.

Reynolds & Begelman (1997) point out that there could be some non-negligible contribution to the reflection line originating even below ISCO. This idea has been put in a more specific context of magnetized accretion flows, as discussed e.g. by Beckwith et al. (2008). On the other hand, Reynolds & Fabian (2008) explored the flow properties close to the black hole and they demostrated that the presence of ISCO leaves a strong imprint on the X-ray reflection spectrum of the accretion disk due to the rapid increase in ionization parameter. Furthermore, Martocchia et al. (2002a) conclude, on the basis of the X-ray iron line modeling in GRS 1915+105 microquasar, that the line production is limited to the region above the ISCO. Also Svoboda et al. (2010) found a convincing case for a disk being truncated rather far above the ISCO (this time in a Seyfert 1.5 galaxy IRAS 05078+1626), whereas Turner et al. (2010) suggest that a persistent 5.44 keV feature exhibited by another Seyfert 1 AGN, NGC 4051, could originate from a preferred radius of the order of a few ISCO.

Despite a simple prediction for the radial dependence of the disk emission provided by the standard accretion disk scenario (Novikov & Thorne 1973; Page & Thorne 1974), a realistic emissivity of a spectral line is not well constrained. In this paper we suggest that the function of radial emissivity could be deduced if the line is produced in discrete rings rather than a whole continuous range of radii. Such an assumption is in fact a very realistic one; in the end the smooth radial profile will have to be replaced by a more complicated emissivity law, which will reflect the mechanism generating the line in a patchy disk structure, perhaps originating from episodic accretion events. The formation of detached annuli has been seen also in some models of strongly magnetized plasma disks (Coppi & Rousseau 2006), where they can develop a periodic structure in radius. Although there is still a long way to prove that such structures could emerge in radiation spectra, it is a real possibility that should be tested observationally.

The existence of ring structure could be revealed by future detailed spectroscopy of the spectral line wings. To this end we develop a rigorous method of calculating the expected energy range of a spectral line, taking into account the effects of strong gravity on photons proceeding from the disk to the observer. These photons may follow complicated routes, but we assume that they do not cross the equatorial plane of the black hole and are neither absorbed nor scattered by environment outside the accretion disk. We give accurate extremal shifts over a wide range of parameters.

The adopted setup is relevant for geometrically thin, planar accretion disks. Needless to say, the method will require high energy resolution together with a sufficient number of counts in the observed spectrum. The former condition is achievable with X-ray calorimeters. The latter one imposes a more serious limitation, however, bright Galactic black holes seem to be appropriate sources. Even if an immediate application of the idea is not possible at present, the calculation of the extremal energy shifts is by itself an interesting addition and of practical use in future.

The paper is organized as follows. In Section 2 we introduce the model of nested rings as a representation of the iron line emissivity from such a radially structured disk. In Section 3 we describe the method of calculating the extremal energy shifts. We provide an iterative semi-

analytical solution for the extremal shifts, $g_{\rm max}$ and $g_{\rm min}$, as functions of three parameters: the emission radius $r_{\rm em}$, spin parameter a, and the inclination angle i. In order to demonstrate the dependencies, we show a graphical representation of $g_{\rm max}$ and $g_{\rm min}$ in terms of parametric plots over the three-dimensional parameter space. Finally, in sections 4 and 5 we discuss and summarize our results.

2. RELATIVISTIC LINE AS SUPERPOSITION OF RING PROFILES

Relativistic spectral lines have been modeled via various approaches, analytical and numerical ones. But one may also ask a simpler question about the extremal energy shifts, which basically give only the line width and the position of the two horns rather than a detailed spectral shape. A double-horn spectral profile is a specific feature of a ring positioned at a given radius. Although the calculation providing just the extremal shifts should seemingly be easy, it has not yet been brought out in a systematic manner.

Fine substructures of the relativistic line from the accretion disk can be used to constrain the inclination angle, radial emissivity distribution in the disk plane, and even the angular momentum of the central black hole (Beckwith & Done 2004). Figure 1 illustrates this by showing the formation of a model spectrum originating as a superposition of several ring profiles. Blue and red horns of the separate rings rise up above the central body of the line. They can be recognized in the wings of the total profile (relative normalization of the rings fluxes has been set proportional to r^{-3}). Sharp peaks of the spectral profile from a narrow ring occur at the maximum and minimum values of the observed energy.

Let us note that the idea of studying the signatures of black holes via spectroscopy of radiation sources in relativistic orbital motion has a long history (Cunningham & Bardeen 1973). Theoretical light curves and spectral line profiles were calculated including various effects of general relativity: the frame-dragging, extreme light-bending, and multiple images (Kojima 1991; Laor 1991; Karas et al. 1992; Matt et al. 1993; Fanton et al. 1997, and further references cited therein).

We concentrate on direct evaluation of the extremal shifts, while the available numerical tools can be used to test our results. To this end, we employ the KY suit of codes (Dovčiak et al. 2004b), which includes KYRLINE routine for the desired observed shape of a relativistic line. In order to achieve high accuracy of simulated lines from very narrow annuli ($\Delta r \lesssim 0.1$), we found the KYRLINE code to be superior in the sense that the resulting profiles do not contain artificial numerical oscillations.[1] This high accuracy is important for understanding the interplay of general relativistic effects (energy shifts and the light bending) that form the spectral profile, because the final shape is more complicated than a simple special-relativistic double-horn line.

3. EXTREMAL ENERGY SHIFTS FROM A RING

3.1. *Light rays as null geodesics*

We consider a spectral line originating from the surface of a geometrically thin, optically thick (standard) accretion disk (e.g., Frank et al. 2002). Propagation of photons from the disk is treated in the limit of geometrical optics in Kerr metric (Misner et al. 1973).[2]

Geodesic motion is determined by three constants of motion: the total energy $\mathcal{E}$, the azimuthal component of angular momentum $L_{\rm z}$, and Carter's constant Q. For photons, null geodesics are relevant, and for them the number of free constants can be further reduced by renormalizing L_z and Q with respect to energy: $\lambda = L_z/\mathcal{E}$, $q^2 = Q/\mathcal{E}^2$. For photons propagating from the accretion disk towards a distant observer, the initial point is set at a given radius in the equatorial plane of the black hole, whereas the final point is at radial infinity, along the view angle of the observer.

Carter's equations for light rays can be written in the integral form (Carter 1968),

$$\int_r \frac{{\rm d}r}{\sqrt{R(r,\lambda,q^2)}} = \pm \int_\mu \frac{{\rm d}\mu}{\sqrt{\Theta(\mu,\lambda,q^2)}}, \qquad (1)$$

where

$$R(r,\lambda,q^2) = r^4 + (a^2-\lambda^2-q^2)r^2 + 2[q^2+(\lambda-a)^2]r - a^2q^2, \qquad (2)$$

$$\Theta(\mu,\lambda,q^2) = q^2 + (a^2-\lambda^2-q^2)\mu^2 - a^2\mu^4, \qquad (3)$$

$\mu = \cos\theta$, and a is the dimensionless spin of the black hole ($0 \le a \le 1$). The left-hand side of eq. (1) describes the motion in radial coordinate, while the right-hand side concerns the latitudinal motion. These equations can be integrated in terms of elliptic integrals (e.g., Rauch & Blandford 1994; Čadež et al. 1998). Roots of polynomials $R(r)$ and $\Theta(\mu)$ correspond to turning points in the radial and latitudinal directions, respectively.

The radial polynomial can be expressed in the form $R = (r-r_1)(r-r_2)(r-r_3)(r-r_4)$, where

$$r_{1,2} = \tfrac{1}{2}F \pm \tfrac{1}{2}D_-^{1/2}, \quad r_{3,4} = -\tfrac{1}{2}F \pm \tfrac{1}{2}D_+^{1/2} \qquad (4)$$

are roots of the polynomial $R(r)$. The latitudinal polynomial adopts the form $\Theta(\mu) = a^2(\mu_-^2+\mu^2)(\mu_+^2-\mu^2)$, with $q^2 > 0$ and the roots

$$\mu_\pm^2 = \frac{1}{2a^2}\left[\left(G^2+4a^2q^2\right)^{1/2} \mp G\right]. \qquad (5)$$

We denoted constants:

$$A \equiv (a^2-\lambda^2-q^2),$$
$$B \equiv (a-\lambda)^2+q^2,$$
$$C \equiv A^2 - 12a^2q^2,$$
$$D \equiv 2A^3 + 72a^2q^2A + 108B^2,$$
$$E \equiv \tfrac{1}{3}\left[(\tfrac{1}{2}E_+)^{1/3} + (\tfrac{1}{2}E_-)^{1/3}\right],$$
$$F \equiv (E - \tfrac{2}{3}A)^{1/2},$$
$$G \equiv \lambda^2 + q^2 - a^2,$$

[1] The code struggles with numerical issues only for infinitesimal rings and very large (edge-on) inclinations, $\Delta r \lesssim 0.01$ and $i \gtrsim 89^{\rm o}$. These limitations do not pose any problem for objects seen at moderate and even rather high inclinations ($i \lesssim 85^{\rm o}$), and the new version of the code (Dovčiak et al., in preparation) improves also these extreme cases.

[2] Hereafter, we express lengths in units of gravitational radius, $r_{\rm g} \equiv GM/c^2 \doteq 1.48 \times 10^{12} M_7$ cm, where M_7 is the mass of the black hole in units of 10^7 solar masses. We use Boyer-Lindquist spheroidal coordinates, (t, r, θ, ϕ).

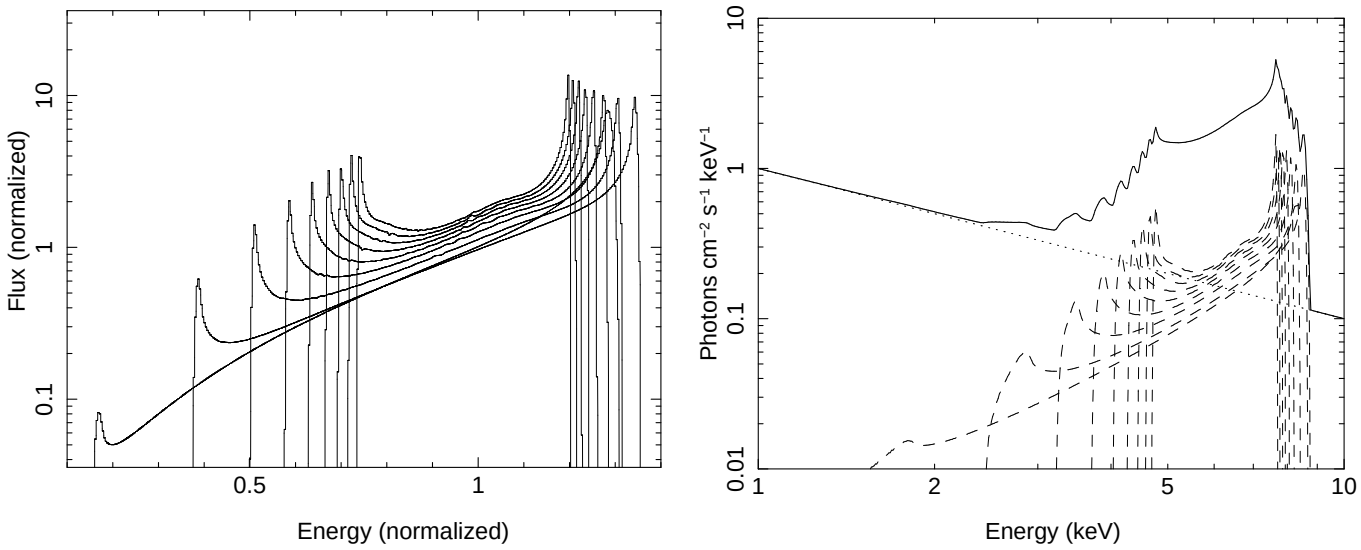

Figure 1. Forming a double-horn spectral line by superposing profiles of several narrow-rings. Left: theoretical profiles from a set of nine infinitesimally narrow rings orbiting in the equatorial plane of a Kerr black hole. Radii of the rings increase equidistantly from $r = 2$ to $r = 18$ gravitational radii. Broader and more redshifted profiles correspond to smaller rings, which rotate at faster speed and reside deeper in the gravitational well. Energy is normalized to the unit rest energy of the line; each profile then extends from $g_{\rm min}$ to $g_{\rm max}$ for its corresponding parameters. Background continuum is subtracted. Right: as on the left, but with rings of a small (finite) radial extent of $\Delta r = 1$. The rest energy of the line is set to 6.4 keV and a power-law continuum added to reflect the fact that line profiles in real spectra are obtained by considering the proper underlying continuum. Dashed lines denote the individual components forming the prototypical spectrum; the latter is shown by the solid line. The signature of the individual rings is visible in the wings of the final profile. The common parameters of both plots are: observer inclination 75° (i.e. close to the edge-on view), black hole spin $a = 0.998$ (prograde rotation).

with $D_\pm = -\frac{4}{3}A - E \pm 4BF^{-1}$, and $E_\pm = D \pm (D^2 - 4C^3)^{1/2}$.

3.2. *Photon energy on arrival to observer*

The energy shift is defined as ratio of observed $E_{\rm o}$ to emitted $E_{\rm e}$ photon energy

$$g = \frac{E_{\rm o}}{E_{\rm e}}. \tag{6}$$

The emission source orbits with four-velocity $\boldsymbol{u} = u^t(1, 0, 0, \Omega)$, where

$$u^t = \left[1 - 2r_{\rm e}^{-1}\left(1 - a\Omega\right)^2 - \left(r_{\rm e}^2 + a^2\right)\Omega^2\right]^{-1/2}, \tag{7}$$

with $\Omega(r_{\rm e}) = (r_e^{3/2} + a)^{-1}$. Introducing the angular velocity into eq. (6), the energy shift is

$$g = \frac{1}{u^t}\frac{1}{1 - \lambda\Omega}. \tag{8}$$

We look for extremal values of the function (8). The definition domain of the energy shift as a function of specific angular momentum, $g(\lambda)$, is an interval $(\lambda_{\rm min}, \lambda_{\rm max})$, which is constrained by the condition of photon reaching the observer.

Even though the equations of the previous section are fairly well known and were discussed in various papers, the extremes of the redshift function g are not so easy to write in an analytical way. Let us remark that an elegant way of determining the energy shifts was derived by Schee et al. (2005) in terms of the light emission loss cone. However, their approach allows only to find the extremal energy shifts of *all* photons emitted from the source at a given position. This includes also those which follow indirect light rays and cross the disk plane. Although the family of direct light rays have generally a simpler shape than the indirect rays, the additional condition prevents us from using the loss cone method to determine the range of energy shifts for a source in the accretion disk.

Only certain combinations of roots and turning points are relevant for light rays involved in our discussion, i.e. those starting from the equatorial ring and reaching a given observer, not crossing the equatorial plane for the second time (we assume that the rays crossing the equatorial plane are obstructed by the disk). We obtain the following combinations.

THE RADIAL INTEGRAL, FOUR REAL ROOTS.

We find

$$\int_{r_{\rm e}}^{\infty} \frac{{\rm d}r}{\sqrt{R(r)}} = g_r\big[F(\varphi_{\rm o}, k_r) \pm F(\varphi_{\rm e}, k_r)\big], \tag{9}$$

where $F(\varphi, k_r)$ is the elliptical integral of the first kind (Byrd & Friedman 1971),

$$\begin{aligned}
g_r(\lambda, q^2) &= 2(r_1 - r_3)^{-1/2}(r_2 - r_4)^{-1/2},\\
k_r(\lambda, q^2) &= \frac{(r_2 - r_3)(r_1 - r_4)}{(r_1 - r_3)(r_2 - r_4)},\\
\varphi_{\rm o}(\lambda, q^2) &= \arcsin\left(\frac{r_2 - r_4}{r_1 - r_4}\right)^{1/2},\\
\varphi_{\rm e}(\lambda, q^2) &= \arcsin\left[\frac{(r_2 - r_4)(r_{\rm e} - r_1)}{(r_1 - r_4)(r_{\rm e} - r_2)}\right]^{1/2}.
\end{aligned}$$

The upper sign in eq. (9) refers to the case of light rays passing through a turning point in the radial direction;

the lower sign refers to those with no radial turning point.

THE RADIAL INTEGRAL, TWO COMPLEX ROOTS.

We set $r_{1,2} = u \pm \mathrm{i}v$ to denote the complex roots, and $r_{3,4}$ to be the real roots. Then, $u = \frac{1}{2}F$, $v = \frac{1}{2}|D_-|^{1/2}$. The radial integral adopts the form

$$\int_{r_\mathrm{e}}^{\infty} \frac{\mathrm{d}r}{\sqrt{R(r)}} = g_r\big[F(\varphi_\mathrm{o}, k_r) - F(\varphi_\mathrm{e}, k_r)\big], \tag{10}$$

where

$$\begin{aligned}
g_r(\lambda, q^2) &= A_c^{-1/2} B_c^{-1/2},\\
k_r(\lambda, q^2) &= \frac{(A_c + B_c)^2 - (r_3 - r_4)^2}{4 A_c B_c},\\
\varphi_\mathrm{o}(\lambda, q^2) &= \arccos\left[\frac{A_c - B_c}{A_c + B_c}\right],\\
\varphi_\mathrm{e}(\lambda, q^2) &= \arccos\left[\frac{(A_c - B_c) r_\mathrm{e} + r_3 B_c - r_4 A_c}{(A_c + B_c) r_\mathrm{e} - r_3 B_c - r_4 A_c}\right],\\
A_c(\lambda, q^2) &= \left[(r_3 - u)^2 + v^2\right]^{1/2},\\
B_c(\lambda, q^2) &= \left[(r_4 - u)^2 + v^2\right]^{1/2}.
\end{aligned}$$

THE LATITUDINAL INTEGRAL.

The latitudinal integral can be written in the form

$$\int_0^{\mu_\mathrm{e}} \frac{\mathrm{d}\mu}{\sqrt{\Theta(\mu, \lambda, q^2)}} = \frac{g_\mu}{a} F(\psi, k_\mu), \tag{11}$$

assuming that the light ray has no latitudinal turning point. Otherwise, the appropriate form of the integral is

$$\int_0^{\mu_\mathrm{e}} \frac{\mathrm{d}\mu}{\sqrt{\Theta(\mu, \lambda, q^2)}} = \frac{g_\mu}{a}[2K(k_\mu) - F(\psi, k_\mu)], \tag{12}$$

where

$$\begin{aligned}
g_\mu(\lambda, q^2) &= (\mu_+^2 + \mu_-^2)^{-1/2},\\
k_\mu(\lambda, q^2) &= \mu_+^2\,(\mu_+^2 + \mu_-^2)^{-1},\\
\psi(\lambda, q^2) &= \arcsin\left[\frac{\mu_\mathrm{o}^2(\mu_+^2 + \mu_-^2)}{\mu_+^2(\mu_\mathrm{o}^2 + \mu_-^2)}\right]^{1/2},
\end{aligned}$$

and $K(k_\mu) = F(\frac{\pi}{2}, k_\mu)$.

3.3. *Iterative solution for extremal shifts*

We search for the extremal values g_min, g_max of the redshift function (8), under a simultaneous constraint by eq. (1). Lagrange multipliers provide a suitable strategy for finding the constrained extremal values. To this end, the multipliers α are defined by the relation

$$\begin{aligned}
\Lambda(\lambda, q^2, \alpha) = \frac{1}{u^t}\frac{1}{1 - \lambda\Omega} &- \alpha \int_{r_\mathrm{e}}^{\infty} \frac{\mathrm{d}r}{\sqrt{R(r, \lambda, q^2)}}\\
&+ \alpha \int_0^{\mu_\mathrm{o}} \frac{\mathrm{d}\mu}{\sqrt{\Theta(\mu, \lambda, q^2)}},
\end{aligned} \tag{13}$$

where partial derivatives of the Lagrange function $\Lambda(\lambda, q^2, \alpha)$ with respect to λ, q^2 and α must vanish identically. The latter condition yields two coupled equations for the unknowns λ and q^2,

$$f_1 = \int_{r_\mathrm{e}}^{\infty} \frac{\mathrm{d}r}{\sqrt{R(r, \lambda, q^2)}} - \int_0^{\mu_\mathrm{o}} \frac{\mathrm{d}\mu}{\sqrt{\Theta(\mu, \lambda, q^2)}} = 0, \tag{14}$$

and

$$\begin{aligned}
f_2 = \frac{\partial f_1}{\partial q^2} = \frac{\partial}{\partial q^2}\Bigg[&\int_{r_\mathrm{e}}^{\infty} \frac{\mathrm{d}r}{\sqrt{R(r, \lambda, q^2)}}\\
&- \int_0^{\mu_\mathrm{o}} \frac{\mathrm{d}\mu}{\sqrt{\Theta(\mu, \lambda, q^2)}}\Bigg] = 0.
\end{aligned} \tag{15}$$

The value of λ conforming to eqs. (14)–(15) corresponds to the desired extremes of the energy shift.

In order to evaluate the extremal values of g, we solve the set (14)–(15) using the Newton-Raphson method. To this end we write Taylor expansion about the root neighborhood,

$$\begin{aligned}
f_1(\lambda, q^2) = 0 = f_1(\lambda_\mathrm{n}, q_\mathrm{n}^2) &+ (\lambda - \lambda_\mathrm{n})\frac{\partial f_1}{\partial \lambda}(\lambda_\mathrm{n}, q_\mathrm{n}^2)\\
&+ (q^2 - q_\mathrm{n}^2)\frac{\partial f_1}{\partial q^2}(\lambda_\mathrm{n}, q_\mathrm{n}^2)\\
&+ \mathcal{O}(\lambda - \lambda_\mathrm{n})^2 + \mathcal{O}(q^2 - q_\mathrm{n}^2)^2,
\end{aligned} \tag{16}$$

$$\begin{aligned}
f_2(\lambda, q^2) = 0 = f_2(\lambda_\mathrm{n}, q_\mathrm{n}^2) &+ (\lambda - \lambda_\mathrm{n})\frac{\partial f_2}{\partial \lambda}(\lambda_\mathrm{n}, q_\mathrm{n}^2)\\
&+ (q^2 - q_\mathrm{n}^2)\frac{\partial f_2}{\partial q^2}(\lambda_\mathrm{n}, q_\mathrm{n}^2)\\
&+ \mathcal{O}(\lambda - \lambda_\mathrm{n})^2 + \mathcal{O}(q^2 - q_\mathrm{n}^2)^2,
\end{aligned} \tag{17}$$

where n is the order of the expansion (to be determined by the desired accuracy of the solution). We define $\Delta\lambda_\mathrm{n} = \lambda - \lambda_\mathrm{n}$ and $\Delta q_\mathrm{n}^2 = q^2 - q_\mathrm{n}^2$ to obtain two relations for $\Delta\lambda_\mathrm{n}$ and Δq_n^2,

$$\Delta\lambda_\mathrm{n}\frac{\partial f_1}{\partial \lambda}(\lambda_\mathrm{n}, q_\mathrm{n}^2) + \Delta q_\mathrm{n}^2 \frac{\partial f_1}{\partial q^2}(\lambda_\mathrm{n}, q_\mathrm{n}^2) \approx -f_1(\lambda_\mathrm{n}, q_\mathrm{n}^2), \tag{18}$$

$$\Delta\lambda_\mathrm{n}\frac{\partial f_2}{\partial \lambda}(\lambda_\mathrm{n}, q_\mathrm{n}^2) + \Delta q_\mathrm{n}^2 \frac{\partial f_2}{\partial q^2}(\lambda_\mathrm{n}, q_\mathrm{n}^2) \approx -f_2(\lambda_\mathrm{n}, q_\mathrm{n}^2), \tag{19}$$

where

$$\Delta q_\mathrm{n}^2 = \frac{f_1\, f_{2,\lambda} - f_2\, f_{1,\lambda}}{f_{1,\lambda}\, f_{2,q^2} - f_{1,q^2}\, f_{2,\lambda}}, \tag{20}$$

$$\Delta\lambda_\mathrm{n} = \frac{-f_1 - \Delta q_\mathrm{n}^2\, f_{1,q^2}}{f_{1,\lambda}}. \tag{21}$$

Eqs. (18)–(19) are linear in $\Delta\lambda_\mathrm{n}$ and Δq_n^2. The solution can be found by successive iterations,

$$\lambda_{\mathrm{n}+1} = \lambda_\mathrm{n} + \Delta\lambda_\mathrm{n}, \quad q_{\mathrm{n}+1}^2 = q_\mathrm{n}^2 + \Delta q_n^2. \tag{22}$$

Results are plotted in Figures 2–4, where we show the extremal shifts as a function of the two main parameters: (i) dimensionless spin of the black hole ($0 \le a \le 1$); and (ii) emission radius r_em of the ring ($r_\mathrm{ms} \le r_\mathrm{em}$, expressed in units of gravitational radii). The inclination angle i

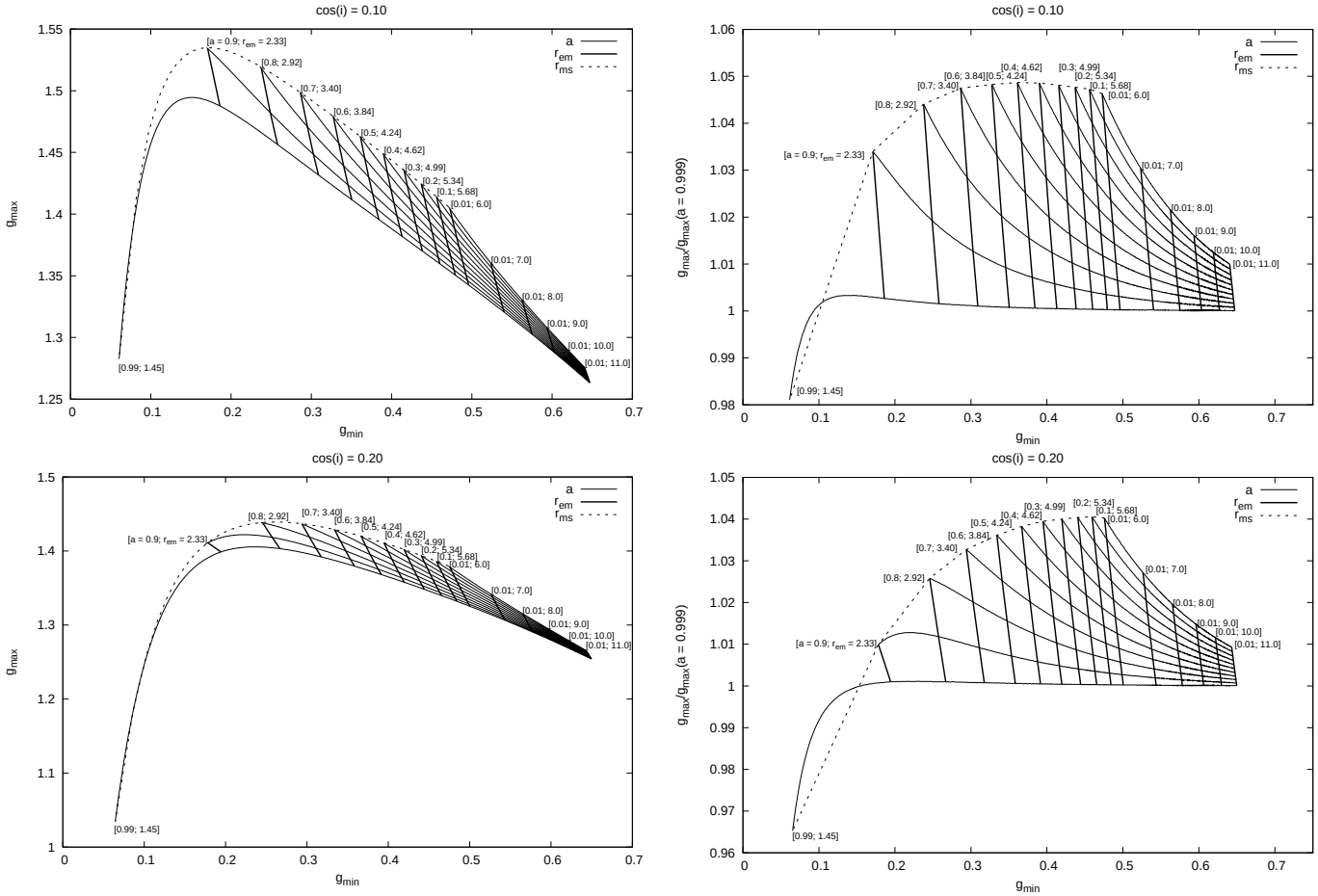

Figure 2. Extremal shifts of the observed photon energy for different view angles of the observer ($\cos i$, given on top of each panel). Left panels: The magnitude of $g_{\rm max}$ versus $g_{\rm min}$. Right panels: As on the left but showing the normalized values on the ordinate (for better clarity of the plot, especially at lower inclinations). Each pair of $g_{\rm max}$, $g_{\rm min}$ values gives the corresponding emission radius $r_{\rm em}$ and the black hole spin a. Curves of constant $r_{\rm em}$ and the spin a are distinguished by different line width (the values are written in brackets). ISCO radius $r = r_{\rm ms}$ defines one boundary of the plot (dotted curve). See the text for details.

stands as a third parameter, which we keep fixed in each of the figures (see the cosine of inclination on top of each panel, $0 \leq i \leq 90^{\rm o}$; edge-on view of the disk corresponds to $i = 90^{\rm o}$).

The behavior of the curves is determined by the interplay of Doppler effect, strong-gravity lensing, and light aberration near the black hole. By increasing r (with a and i fixed) both $g_{\rm min}$ and $g_{\rm max}$ increase when i is small, showing that the dominant factor is the gravitational redshift rather than the relativistic beaming. On the other hand, the latter becomes important for large inclinations.

The method of solution is efficient enough and it allows us to explore parameters in a systematic way. On the other hand, because the parameter space is quite rich and the plots contain wealth of information, one may need to get accustomed to the actual meaning of the presented curves. Broadly speaking, the approaching side of the ring produces photons around $g_{\rm max}$ energy, whereas the receding part gives $g_{\rm min}$ for the given radius and spin. These trends are further influenced by the overall gravitational redshift, which eventually prevails as the emission radius approaches the horizon, and the light bending effect, which enhances the signal from a region of the disk around the radiation caustic at high view angles.

We remind the reader, that the extremal shifts $g_{\rm min}$ and $g_{\rm max}$ play a *role of observable quantities*. It is convenient to have them given directly on the axes. Given $g_{\rm min}$, $g_{\rm max}$ one can immediately find the corresponding values of the emission radius and the black hole spin. The set of Figures 2–4 covers the parameter values usually considered when modeling the accreting black hole sources, i.e. the emission originating from near above the ISCO.

We also constructed the normalized plots, where $g_{\rm max}(a)$ on the ordinate is divided by its value for $a = 0.999$. These graphs are given in the right panels of Figures 2–3 for comparison with the unnormalized graph for high inclinations ($\cos i \lesssim 0.4$) in left panels. For lower inclinations we give only normalized graphs ($\cos i \gtrsim 0.5$; Figure 4) because in this case the dependence on the spin is very weak.

Finally, the normalized graphs are supplemented by Figure 5, which has been constructed just for the fixed value of $a = 0.999$. It allows us to read the normalization factor and to reconstruct the absolute values of the extremal shift in previous plots.

4. DISCUSSION

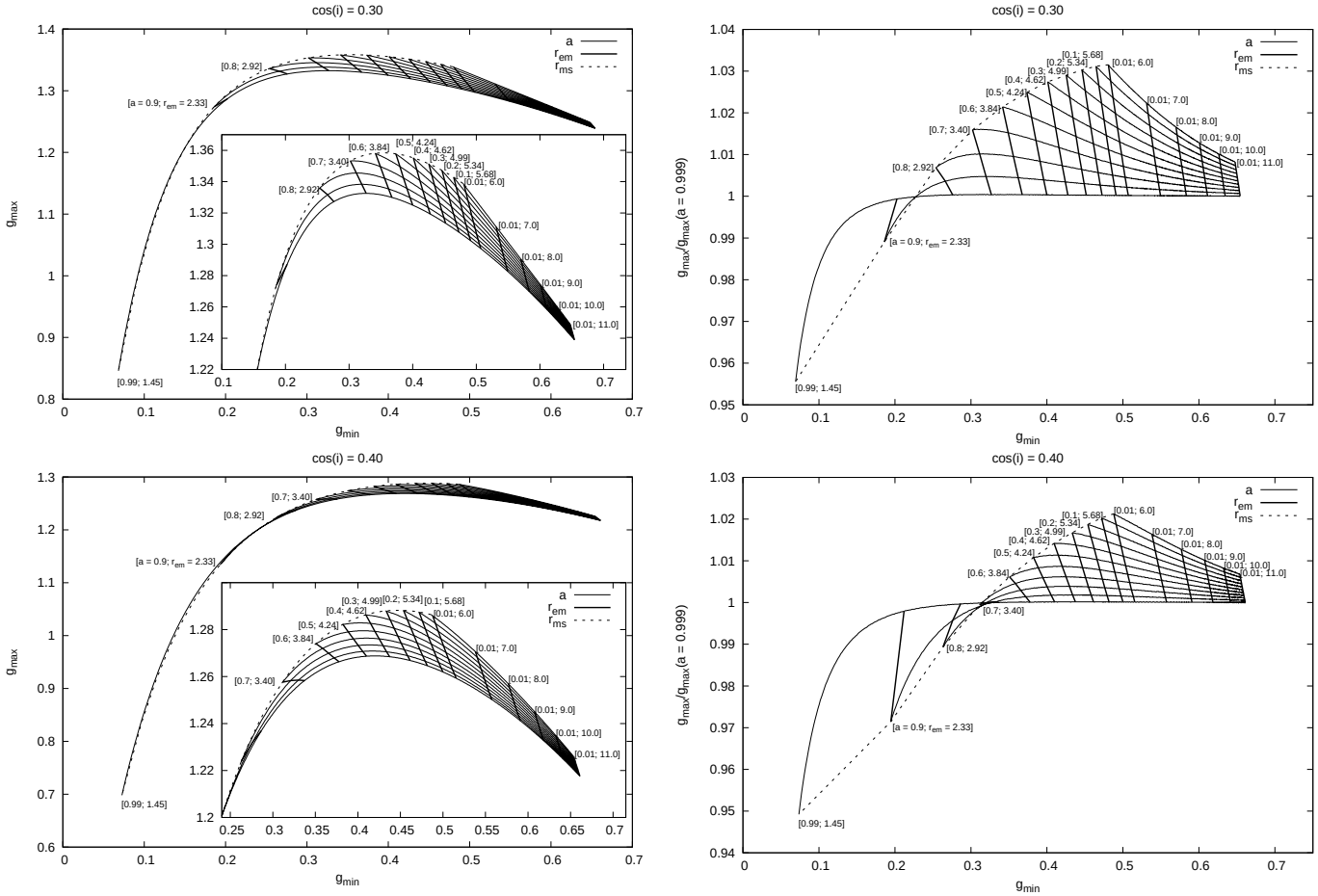

Figure 3. As in the previous figure, but for lower inclination angles. By decreasing the inclination the dependency on the black hole spin becomes less prominent, and so the curves for different a get closer to each other. Therefore, in the left column we show an inset where the relevant part of the plot is enlarged.

Wings of the relativistic line become more complex when the outgoing signal is integrated over a finite range of radii. This is also the case of the aggregate line profile that has been frequently considered as originating from a radially extended zone of an accretion disk. According to the relativistic version of the standard disk model the emissivity has a maximum near above the ISCO and it falls down towards the inner rim as well as towards infinity, however, the dissipation in a hot corona does not need to follow this law. Therefore, the line radial emissivity cannot be inferred solely from the standard disk model. Part of the information from the spectral profile is lost in the radially integrated spectrum.

How could the extremal shifts be used to reconstruct, at least in principle, the putative rings forming the spectral line radial emissivity profile? The main underlying assumption requires that the horns are resolved in the total observed profile. In fact, the right panel of Figure 1 exhibits the individual components, which are summed to form the final line profile. Each of these partial constituents corresponds to one elementary ring, radius of which can be read from the $g_{\rm max}$ vs. $g_{\rm min}$ graph. In this way the observed profile can be decomposed into the components. The required time resolution of the method is of the order of orbital time at the innermost ring.[3] We further assumed that an independent constraint on the disk inclination angle can be given. This can be based for example on the ratio of equivalent widths of the two horns. Then one will be able to read the emission radius and the black hole spin from our graphs. Or, instead of the graphical method, a fitting procedure can be employed using pre-computed tables of the energy shifts.

Naturally, this decomposition of an accretion disk into rings does not distinguish between the case of almost steady rings versus transient features that exist for a shorter period of time. The two cases should produce the same orbit-integrated profiles, so in this respect the assumption about the ring structure stands in the basis of our method. This was discussed in more detail by Czerny et al. (2004), who had developed an approximation for the mean spectra of transient flares, which they treat in terms of "belts" representing the time-averaged traces of the flares on the disk surface. This scheme produces the ring structure of the reflection spectra of the line emission fully consistent with the picture adopted in the current paper.

We note that another approach to the problem of constraining the radial emissivity of the iron line, by well-resolved time-independent spectral profiles, was discussed by Čadež et al. (2000), or by using the hot-spot

[3] Keplerian orbital time as function of radius and spin of Kerr black hole is given by $T_{\rm orb}(r;M,a) \doteq 310\ \left(r^{\frac{3}{2}}+a\right)\frac{M}{10^7 M_\odot}$ [sec].

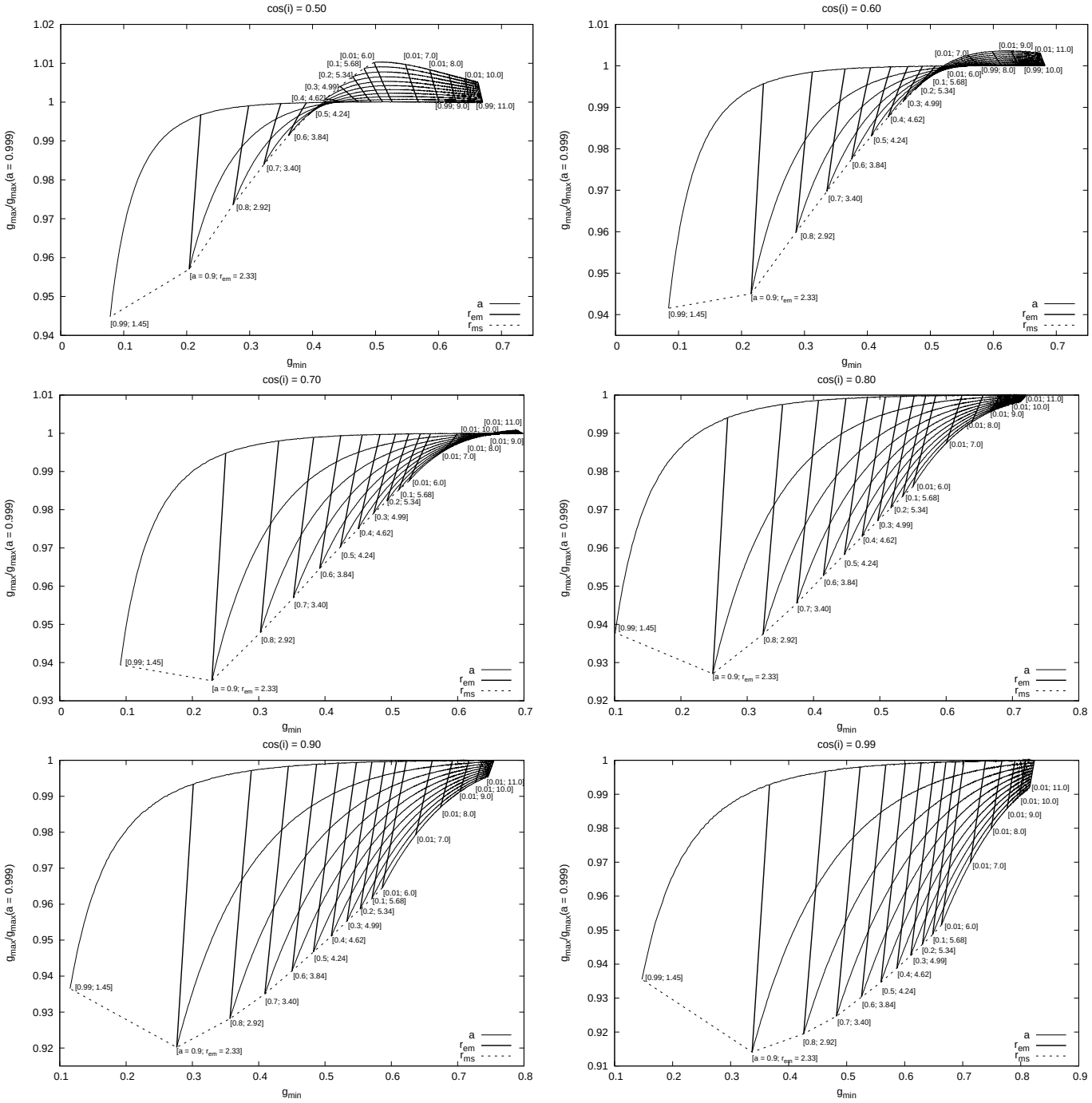

Figure 4. Normalized graphs of $g_{\max}$ vs. $g_{\min}$ for low inclinations, i.e. close to the face-on view of the disk plane. Bottom-right panel corresponds to the view of the disk along the rotation axis.

scenario by Murphy et al. (2009). However, the currently available data do not allow us to achieve the high time resolution necessary to reveal the individual orbiting spots in AGNs; this would require to study time-scales of the order of $T_{\rm orb}$, which is for supermassive black holes typically $\sim 10^3$ sec and shorter. Therefore, significantly higher collecting area is needed. Alternatively one could apply this approach to accreting Galactic (stellar) black holes, which can be brighter. In fact, the relativistic iron line has been measured in several stellar black holes – e.g. the case of GRS 1915+105 microquasar (Martocchia et al. 2002b), or see the recent discussion of XTE J1550-564 microquasar (Steiner et al. 2010, and references cited therein). However, in the case of stellar-mass black holes the time-scales are expected to be shorter, as follows from the mass-scaling relation.

The above-mentioned approaches offer a potentially interesting application (though neither is useful in the context of present data). Either significantly higher numbers of photon counts are required, or one needs to catch the accretion disk in a state when a very small number of well-separated annuli dominate the line emission, so that the two different annuli of the accretion disk can be distinguished from each other.

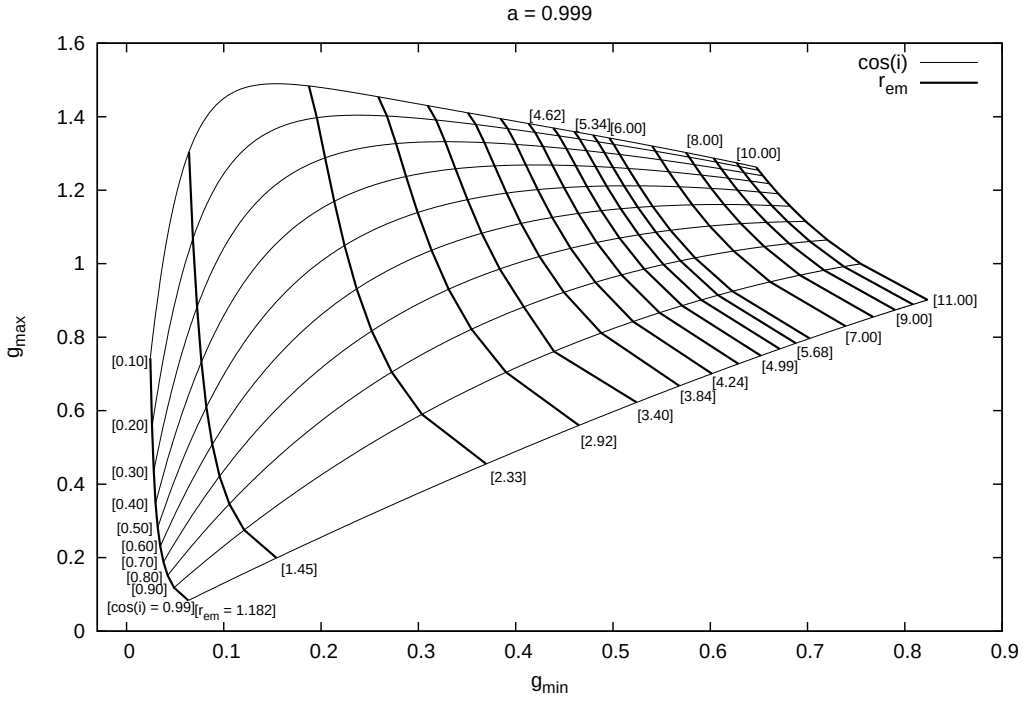

Figure 5. Extremal energy shift for $a = 0.999$. Set of contours of constant inclination angle and of constant emission radius are shown. This plot gives the scaling factor $g_{\max}(a = 0.999)$ of the normalized graphs in Figures 2–4.

5. CONCLUSIONS

Calculation of the extremal energy shifts in Section 3 and their graphical representation in Figures 2–4 are the main results of the paper. The principal assumption of the proposed application is about discrete rings forming the line emission. Knowing the extremal shifts can be useful also in another context, namely, the narrow (emission) lines produced by orbiting transient flares and spots on the accretion disk surface (Dovčiak et al. 2004a; De Marco et al. 2009). Given the intrinsic emission energy, the extremal energy shifts define the range where these spectral features can appear in the observed spectrum.

We examined theoretical profiles of the relativistic spectral line emerging from a set of concentric narrow rings which, as a whole, form a radially extended zone of an inner accretion disk. In particular we developed a systematical approach to determine the maximum and minimum energy shifts of the observed line as a function of the model parameters. As a motivation for our study we have mentioned non-monotonic radial profiles of emissivity that are consistent with intermittent episodes of accretion, and models of magnetized plasma rings with radially periodic structure.

We constrained our calculations to photons arriving along direct light rays, i.e., we ignored the higher-order images that could arise by rays making several revolutions around the black hole. This constraint is well-substantiated: firstly because the flux in these indirect images decreases exponentially with the image order ($n = 2, 3, \ldots$), and secondly these images are anyway blocked by the accretion disk.

We also neglected some other complications, such as the role of obscuration, the impact of geometrically thick (non-planar) shape of the accretion disk, or its warping. We expect that for example the role of source covering by intervening clouds along the line of sight (Karas et al. 2000) will not affect the results although it could make the proposed method more difficult by enhancing the fluctuations of the observed signal. In case of AGN, the role of accretion disk self-gravity can be important as it can significantly affects the vertical height of the outer regions of the disk (Karas et al. 2004). These effects should be considered in a future work.

We thank M. Dovčiak, G. Matt and T. Pecháček for helpful discussions. We acknowledge the Czech Science Foundation program (refs. 205/07/0052 and 205/09/H033) and the European Space Agency PECS no. 98040. The Astronomical Institute is supported by the Center for Theoretical Astrophysics (LC06014).

REFERENCES

Beckwith, K., & Done, C. 2004, MNRAS, 352, 353
Beckwith, K., Hawley, J. F., & Krolik, J. H. 2008, ApJ, 390, 21
Byrd, P. F., & Friedman, M. D. 1971, Handbook of Elliptic Integrals for Engineers and Scientists (New York: Springer-Verlag)
Čadež, A., Calvani, M., di Giacomo, C., & Marziani, P. 2000, New Astronomy, 5, 69
Čadež, A., Fanton, C., & Calvani, M. 1998, New Astronomy, 3, 647
Carter, B. 1968, Phys. Rev., 174, 1559
Coppi, B., & Rousseau, F. 2006, ApJ, 641, 458
Cunningham, C. T., & Bardeen, J. M., 1973, ApJ, 183, 273
Czerny, B., Różańska, A., Dovčiak, M., Karas, V., & Dumont, A.-M. 2004, A&A, 420, 1
De Marco, B., Iwasawa, K., Cappi, M., Dadina, M., Tombesi, F., Ponti, G., Celotti, A., & Miniutti, G. 2009, A&A, 507, 159
Dovčiak, M., Bianchi, S., Guainazzi, M., Karas, V., & Matt, G. 2004a, MNRAS, 350, 745
Dovčiak, M., Karas, V., & Yaqoob, T. 2004b, ApJSS, 153, 205

Fabian, A. C., Iwasawa, K., Reynolds, C. S., & Young, A. J. 2000, PASP, 112, 1145
Fanton, C., Calvani, M., de Felice, F., & Čadež, A. 1997, PASJ, 49, 159
Frank J., King A., & Raine D. 2002, Accretion Power in Astrophysics (Cambridge: Cambridge University Press)
Karas, V., Czerny, B., Abrassart, A., & Abramowicz, M. A. 2000, MNRAS, 318, 547
Karas, V., Huré, J.-M., Semerák, O. 2004, Classical and Quantum Gravity, 21, R1
Karas, V., Vokrouhlický, D., & Polnarev, A. G. 1992, MNRAS, 259, 569
Kojima, Y. 1991, MNRAS, 250, 629
Laor, A. 1991, ApJ, 376, 90
Martocchia, A., Matt, G., & Karas, V. 2002a, A&A, 383, 23
Martocchia, A., Matt, G., Karas, V., Belloni, T., & Feroci, M. 2002b, A&A, 387, 215
Matt, G., Perola, G. C., & Stella, L. 1993, A&A, 267, 643
McClintock, J. E., & Remillard, R. A. 2006, in: Compact Stellar X-ray Sources, eds. W. Lewin & M. van der Klis (Cambridge: Cambridge University Press), pp. 157–213
Miller, J. 2007, ARA&A, 45, 441
Miller, J. M., Fabian, A. C., Wijnands, R., Remillard, R. A., & Wojdowski, P., Schulz, N. S., Di Matteo, T., Marshall, H. L., Canizares, C. R., Pooley, D., & Lewin, W. H. G. 2002, ApJ, 578, 348
Misner, C. W., Thorne, K. S., & Wheeler, J. A. 1973, Gravitation (New York: W. H. Freeman & Co)
Murphy, K. D., Yaqoob, T., Karas V., & Dovčiak M. 2009, ApJ, 701, 635
Novikov, I. D., & Thorne K. S. 1973, in Black Holes, eds. C. DeWitt and B. S. DeWitt (New York: Gordon & Breach), p. 343
Page, D. N., & Thorne, K. S. 1974, ApJ 499, 191
Rauch, K., & Blandford, R. 1994, ApJ, 421, 46
Reynolds, C. S., & Begelman, M. C. 1997, ApJ, 488, 109
Reynolds, C. S., & Fabian, A. C. 2008, ApJ, 675, 1048
Reynolds, C. S., & Nowak, M. A. 2003, Phys. Rep., 377, 389
Schee, J., Stuchlík, Z., & Juráň, J. 2005, in: Black Holes and Neutron Stars, Vol 6/7, eds. S. Hledík and Z. Stuchlík (Opava: Silesian University), pp. 143–155
Steiner, J. F., Reis, R. C., McClintock, J. E., Narayan, R., Remillard, R. A., Orosz, J. A., Gou, L., Fabian, A. C., & Torres, M. A. P. 2010, MNRAS, submitted (arXiv:1010.1013)
Svoboda, J., Guainazzi, M., & Karas, V. 2010, A&A, 512, id. A62
Turner, T. J., Miller, L., Reeves, J. N., Lobban, A., Braito, V., Kraemer, S. B., & Crenshaw, D. M. 2010, ApJ, 712, 209